Topological Nernst Effect of the Two-Dimensional Skyrmion Lattice

Max Hirschberger,[1,2,*] Leonie Spitz,[1,†] Takuya Nomoto,[2] Takashi Kurumaji,[1,‡] Shang Gao,[1,§] Jan Masell,[1] Taro Nakajima,[1,‖] Akiko Kikkawa,[1] Yuichi Yamasaki,[3,4] Hajime Sagayama,[5] Hironori Nakao,[5] Yasujiro Taguchi,[1] Ryotaro Arita,[2] Taka-hisa Arima,[1,6] and Yoshinori Tokura[1,2,7]

[1]*RIKEN Center for Emergent Matter Science (CEMS), Wako, Saitama 351-0198, Japan*
[2]*Department of Applied Physics and Quantum-Phase Electronics Center, The University of Tokyo, Bunkyo-ku, Tokyo 113-8656, Japan*
[3]*Research and Services Division of Materials Data and Integrated System (MaDIS), National Institute for Materials Science (NIMS), Tsukuba, Ibaraki 305-0047, Japan*
[4]*PRESTO, Japan Science and Technology Agency (JST), Kawaguchi, Saitama 332-0012, Japan*
[5]*Institute of Materials Structure Science, High Energy Accelerator Research Organization, Tsukuba, Ibaraki 305-0801, Japan*
[6]*Department of Advanced Materials Science, The University of Tokyo, Kashiwa, Chiba 277-8561, Japan*
[7]*Tokyo College, The University of Tokyo, Bunkyo-ku, Tokyo 113-8656, Japan*

(Received 8 October 2019; revised 16 May 2020; accepted 10 July 2020; published 12 August 2020)

The topological Hall effect (THE) and its thermoelectric counterpart, the topological Nernst effect (TNE), are hallmarks of the skyrmion lattice phase (SkL). We observed the giant TNE of the SkL in centrosymmetric Gd_2PdSi_3, comparable in magnitude to the largest anomalous Nernst signals in ferromagnets. Significant enhancement (suppression) of the THE occurs when doping electrons (holes) to Gd_2PdSi_3. On the electron-doped side, the topological Hall conductivity approaches the characteristic threshold $\sim 1000\ (\Omega\,\mathrm{cm})^{-1}$ for the intrinsic regime. We use the filling-controlled samples to confirm Mott's relation between TNE and THE and discuss the importance of Gd-5d orbitals for transport in this compound.

DOI: 10.1103/PhysRevLett.125.076602

A skyrmion spin-vortex [1,2] represents a quantized unit of scalar spin chirality $\chi_{\alpha\beta\gamma} = \mathbf{S}_\alpha \cdot (\mathbf{S}_\beta \times \mathbf{S}_\gamma)$, defined for three neighboring magnetic moments on lattice sites α, β, and γ. It was realized early on that spin-winding results in an emergent gauge field acting on moving particles, leading to anomalies such as the topological (or geometrical) Hall effect (THE) and its sibling, the topological Nernst effect (TNE) [3–9]. The relative magnitude of the carrier mean-free path l_{mfp} as compared to the size of the skyrmion λ_{sk}, i.e., to the size of the magnetic unit cell, governs the appropriate starting point for theoretical modeling [10]. Well-known cases of noncentrosymmetric materials with a skyrmion lattice (SkL) phase, such as MnSi [2,11–13], fall into the regime $l_{\mathrm{mfp}} \ll \lambda_{\mathrm{sk}}$, and it is understood that the (weak) THE relates to a Berry-phase induced deflection of wave packets moving through the twisted spin texture in real space [6,13–15]. Meanwhile, the as-yet unexplored "intrinsic" (momentum-space) limit $l_{\mathrm{mfp}} \geq \lambda_{\mathrm{sk}}$ necessitates a modification of the electronic wave functions themselves by the presence of magnetic order, which is predicted to yield a large THE and TNE due to Berry curvature in reciprocal space [5,16–20].

To describe the connection between TNE and THE, we write the electric currents $\mathbf{J}$ emanating from an applied electric field $\mathbf{E}$ or an applied temperature gradient $(-\nabla T)$ as $J_i = \sigma_{ij} E_j$ and $J_i = \alpha_{ij}(-\nabla_j T)$, respectively. The TNE provides insight into the effect of a variation of the chemical potential ζ, as expressed by the Mott relation [21,22]

$$\alpha_{ij}/T = -(\pi^2/3)(k_B^2/e)(\partial\sigma_{ij}/\partial\varepsilon)_{\varepsilon=\zeta}, \qquad (1)$$

where k_B, e (>0), and ε represent the Boltzmann constant, the fundamental charge, and the band filling energy, respectively. Due to experimental constraints—such as relatively weak spin polarization and low skyrmion density in the ambient pressure, equilibrium SkL phases of chiral B20 compounds (skyrmion-skyrmion distance ~20–200 nanometers)—the TNE of a SkL has never hitherto been observed experimentally.

In this Letter, we report the large TNE of the SkL in centrosymmetric Gd_2PdSi_3, compare its magnitude to recently observed giant anomalous Nernst responses in ferromagnets, and show how the TNE is related to the enhancement (decrease) of the THE under electron (hole) doping through the Mott relation. We demonstrate that on the electron-doped side, the intrinsic limit of the THE may be within reach, and that the large transport responses in Gd_2PdSi_3 are likely related to the prevalence of Gd-5d conducting orbitals in close proximity to the Fermi energy.

Rare-earth intermetallics with SkL phase, such as Gd_2PdSi_3 [23], $Gd_3Ru_4Al_{12}$ [24], and $GdRu_2Si_2$ [25] are highly suitable for investigating the transport response

from the emergent gauge field: a tiny vortex-vortex distance $\lambda \sim 2$–3 nm leads to giant responses, strongly modifying the trajectory of moving charge carriers. We focus here on centrosymmetric, hexagonal Gd_2PdSi_3 [Fig. 1(a)], where magnetic long-range order onsets at $T_N \sim 20$ K. The dominant magnetic ion is Gd^{3+} in the triangular lattice plane. Dzyaloshinskii-Moriya interactions, which are intrinsic to noncentrosymmetric material platforms and which favor helical order and skyrmion spin textures, are expected to be globally absent in this centrosymmetric bulk crystal [23]. Instead, skyrmion formation is driven by frustrated interactions mediated through the conduction electrons [26,27] and remarkably, skyrmions were found to exist (for the magnetic field $\mathbf{B} \| c$ axis) even at the lowest $T = 2$ K, i.e., at $T/T_N \sim 0.1$ [23]. Located between two phases with zero net scalar spin chirality [spiral-like IC-1 (possibly multi-$\mathbf{q}$) and the fanlike IC-2, Fig. 1(b)], the topologically stable SkL is bounded by sharp, first-order phase transitions as observed in the strongly hysteretic field-derivative of the magnetization [DC susceptibility χ_{DC}, Fig. 1(d) see also Refs. [23,28]]. This phase alone was found to host enormous THE and TNE responses in our high-resolution transport experiments [Figs. 1(c), 1(e)–1(g), see Supplemental Material for technical details [29]], the Hall signal being in good agreement with previous work [23,28].

We consider cases where Nernst signals arising from noncoplanar spin arrangements have previously been reported: (i) Pyrochlore $Nd_2Mo_2O_7$, a canted ferromagnet where the signal is roughly proportional to the net magnetization at all T studied [62]. (ii) B-20 type, helimagnetic MnGe, where the THE and TNE probe the imbalance between positive and negative contributions to the gauge field. These originate from magnetic monopoles and antimonopoles, respectively [7,63]. (iii) Thin films of the Heusler alloy $Mn_{1.8}PtSn$, the magnetic structure of which was not verified independently [64]. In contrast to these cases, the Nernst effect from the SkL laid out here represents a minimal, textbooklike example of the thermoelectric response emerging from a spin texture with integer winding per magnetic unit cell.

The Nernst conductivity (sometimes referred to as transverse thermoelectric conductivity or transverse Peltier conductivity [29]) is calculated via $\alpha_{xy} = S_{xy}\sigma_{xx} + S_{xx}\sigma_{xy}$, requiring input from the longitudinal thermopower S_{xx} [Fig. 1(e)]. S_{xx} is of comparable magnitude for the two low-field phases IC-1 and SkL; the strong difference of THE and TNE in the respective phases, as well as sharp maxima in χ_{DC} [Fig. 1(d)], clearly distinguish these two states. Figures 1(f) and 1(g) show the experimentally obtained Nernst effect S_{xy}/T and Nernst conductivity α_{xy}/T (entropy factors removed). Note that α_{xy}/T

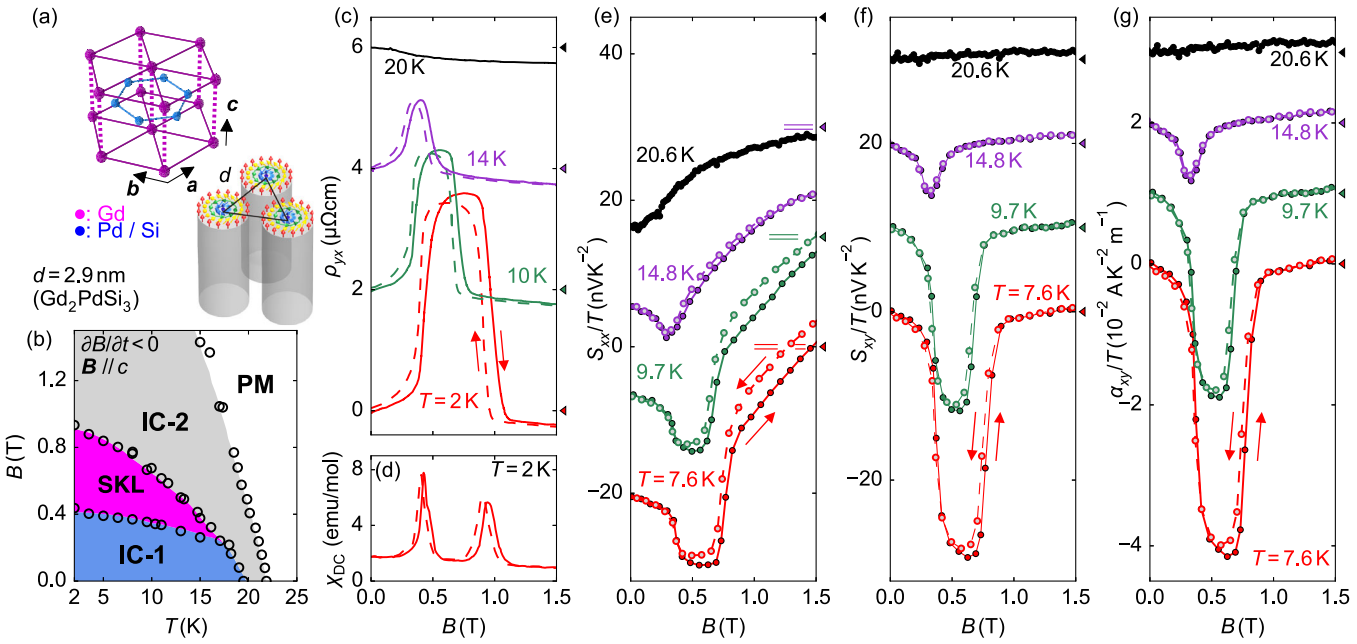

FIG. 1. (a) Hexagonal structure (basic AlB_2-type) of Gd_2PdSi_3. Inset: high-density SkL state with nanometer-sized interskyrmion distance d. (b) Magnetic phase diagram for $\mathbf{B} \| c$ and decreasing field $\partial B/\partial t < 0$, as adapted from Ref. [61]. Labels indicate the IC-1 ground state, the skyrmion lattice phase, the IC-2 fanlike state, and the paramagnetic regime (PM). (c) Hall resistivity, (e) thermopower, (f) Nernst effect, and (g) Nernst conductivity. For the latter three, entropy factor $\sim T$ was removed. (d) Magnetic susceptibility $\chi_{DC}(B)$ at the lowest $T = 2$ K. Curves in panels (c),(e)–(g) were shifted by vertical offsets of 2 $\mu\Omega$ cm, 15 nV K^{-2}, 10 nV K^{-2}, and 0.01 AK^{-2} m^{-1}, respectively. The zero level for each curve is indicated by a colored triangle at the right side of the panel. Solid arrows mark the direction of the field ramp. In (e), red, green, and purple twinned lines also indicate zero levels for $T = 7.6$, 9.7, and 14.8 K.

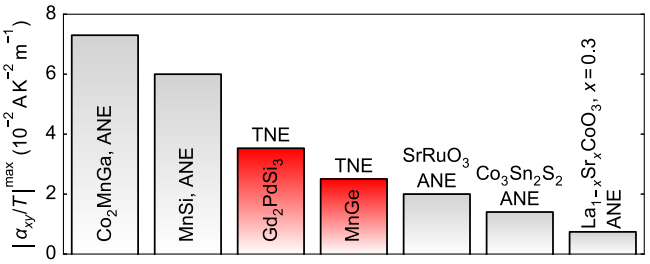

FIG. 2. Comparison of large Nernst conductivity α_{xy}/T driven by magnetic order for various materials reported in the literature. Grey shading indicates anomalous Nernst response (ANE, proportional to the net magnetization M), while red shading is reserved for the topological Nernst effect (TNE, proportional to the scalar spin chirality).

represents the intrinsic transverse thermoelectric response [21], while the derived observable S_{xy} depends strongly on T (via the entropy factor) and the resistivity, i.e., the scattering properties, of the material [65].

For perspective we compare, side-by-side in Fig. 2, representative magnetic materials with anomalous (ANE, i.e., proportional to the net magnetization M) or topological (TNE, proportional to the scalar spin chirality) α_{xy}/T. Although the TNE of Gd_2PdSi_3 cannot match the ultralarge ANE exhibited by the ferromagnetic Weyl semimetal Co_2MnGa [66], it easily outperforms the ANE of more metallic ferromagnets, e.g., $SrRuO_3$ [67] or elemental Fe and Co, for which only sparse data [68] and calculated values [69] are available at present [29].

The large TNE signal with negative sign indicates, from Eq. (1), that significant enhancement of the THE should be observed when moving the chemical potential ζ of Gd_2PdSi_3 upwards. Knowing that Pd-4d orbitals are located about 4 eV below ζ [70], a gentle shift of ζ may be achieved using a series of slightly carrier-doped crystals $Gd_2(Pd_{1-x}M_x)Si_3$ with M = Rh (hole doping) or Ag (electron doping), as shown in Fig. 3. We define a generalized nominal dopant concentration $z = -x$ on the hole-doped and $z = x$ on the electron-doped side. The single crystals were characterized thoroughly using solid state techniques [29]. Figures 3(a) and 3(b) report the ordering temperature T_N from magnetic susceptibility as well as the modulation vector $\mathbf{q} = (q, 0, 0)$ of the ground state from resonant elastic x-ray scattering (REXS) at the Gd-L_2 absorption edge in reflection geometry [sketch in Fig. 3(a)]. We determined q from scans of scattering intensity along high-symmetry lines in momentum space [Fig. 3(b), inset]. These data show that the magnetic properties are but weakly affected by chemical substitution on the Pd site.

In electrical transport measurements, the topological Hall resistivity ρ_{yx}^T changes significantly with z [Figs. 3(c) and 3(d), respectively]. We calculate the topological Hall conductivity $\sigma_{xy}^T = \rho_{yx}^T/(\rho_{xx}^2 + \rho_{yx}^2)$, shown in Fig. 3(e) for selected samples. The peak value $\max[\sigma_{xy}^T(B, T = 2\text{ K})]$ is plotted in Fig. 3(f). The green line in this panel has a slope determined directly from the magnitude of the topological Nernst conductivity α_{xy}^T/T using Eq. (1) [29]. A necessary ingredient of the

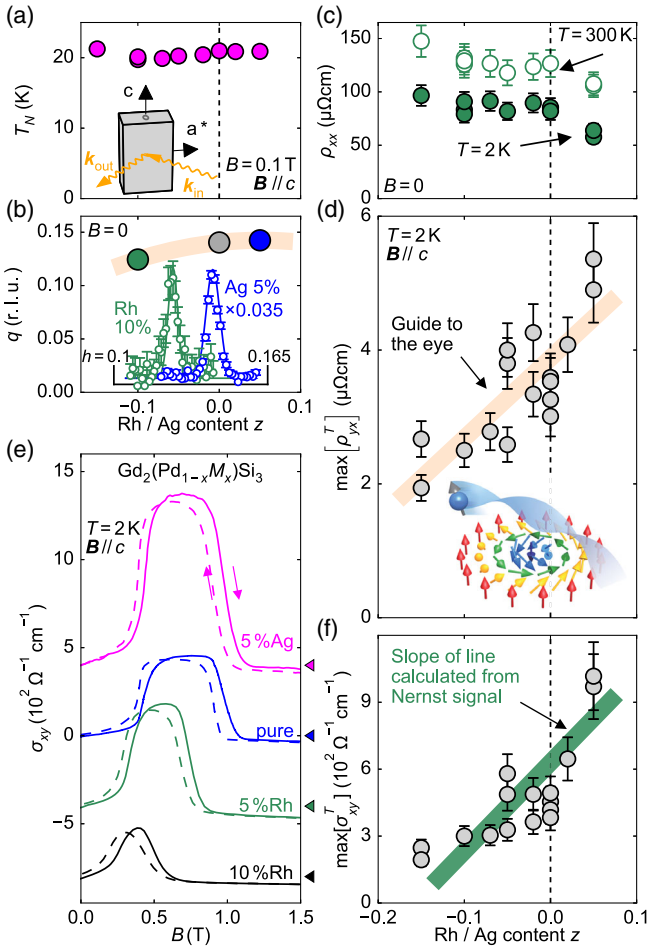

FIG. 3. (a) Néel temperature T_N of $Gd_2(Pd_{1-x}M_x)Si_3$ from magnetic susceptibility. M = Rh, Ag corresponds to $z < 0$ ($z > 0$), respectively (see text). Inset: sample geometry for resonant elastic x-ray diffraction (REXS) at the Gd-L_2 edge in reflection geometry. (b) Magnetic wave number q, determined from REXS. The data point for pure Gd_2PdSi_3 (grey disk) is reproduced from Ref. [23]. Inset: line scans of REXS intensity along $(2 - h, 1, 0)$ in reciprocal space for two samples, after the subtraction of a constant background. The beam energy was set to $E = 7.935$ keV and the sample temperature was $T = 4$ K (5 K) for the Ag-doped (Rh-doped) crystal. Scale of y axis (not shown) is intensity normalized by monitor counts (arbitrary units). Statistical errors of detector counts are indicated. (c) Longitudinal resistivity as well as extremal (d) topological Hall resistivity and (f) topological Hall conductivity. Systematic (sample shape) errors are indicated. In (e), raw data of Hall conductivity as a function of magnetic field. Inset of (d), illustration of the real-space Berry-phase mechanism for the THE and TNE [6,12]. Red lines in (b),(d) are guides to the eye, while the green line in (e) was calculated from the Nernst conductivity (see text). Vertical dashed lines mark $z = 0$.

calculation, the inverse density of states $\partial\varepsilon/\partial z$, was estimated from the specific heat of isoelectronic Y_2PdSi_3 [29,71]. Good agreement of the doping study with the Nernst signal—without any adjustable parameters—amounts to a direct experimental confirmation of Eq. (1) for the THE and TNE.

The combined band filling and thermoelectric experiment establishes Gd_2PdSi_3 as a model material for the quantitative exploration of transport responses in the presence of rather mild changes to the magnetic properties. Note that the Mott relation for the TNE has, to the best of our knowledge, never before been demonstrated in the literature. Even for the ANE, the only test without adjustable parameters was carried out using thin films of $Cr_x(Sb_{1-y}Bi_y)_{2-x}Te_3$, with ferromagnetism induced by dilute Cr spins ($x = 0.15$, Refs. [29,72]). We emphasize that not only can the sign of the filling-induced change to σ_{xy}^T be predicted from α_{xy}^T but even its magnitude to within several tens of percents.

We further scrutinize underlying assumptions made in comparing the TNE with the THE for the doped crystals. First, Eq. (1) describes the regime of linear response. Hence, we note that despite being moderately large ($-\partial_x T \sim 0.3$ K/mm), the longitudinal T gradient in our Nernst experiment on Gd_2PdSi_3 is too small to unpin the SkL, and to result in a flux-flow type Nernst effect [29]. Second, Smrčka and Středa derived Eq. (1) by changing ζ while leaving all other parameters unaffected—such as character of the magnetic ordering, nature of the electronic bands, and scattering processes [22]. We have demonstrated the stability of the magnetic order in Fig. 3 and, because even stoichiometric Gd_2PdSi_3 already has significant residual resistivity, the introduction of dopants does not excessively affect the scattering properties [29]. Third, the electronic spectrum of Gd_2PdSi_3 is sufficiently broadened by disorder to justify the linear approximation [green line in Fig. 3(f)] [29].

It is worth emphasizing that the validity of Mott's relation is in itself experimental evidence for the suitability of the rigid band scenario in describing mild changes of composition in $Gd_2(Pd_{1-x}M_x)Si_3$ ($M = $ Rh, Ag). However, the notion of rigid bands warrants some more careful examination. As a first step, we have calculated the partial density of states (P-DOS) $g_P(\varepsilon)$ of pure Gd_2PdSi_3 in the framework of density functional theory (DFT) [Fig. 4(a)], using the Ce_2CoSi_3 structure type. The calculations were carried out in the fully spin-polarized state (see the Supplemental Material for technical details [29]). Figures 4(b) and 4(c) further illustrate the effect of doping. The size of the unit cell for the doped cases was doubled along c, and one Pd atom was replaced with Rh or Ag [29]. Although this is an imperfect approximation for randomly distributed dopants in the experimental study, shifting of the total density of states (DOS) to the left (right) side for electron (hole) doping

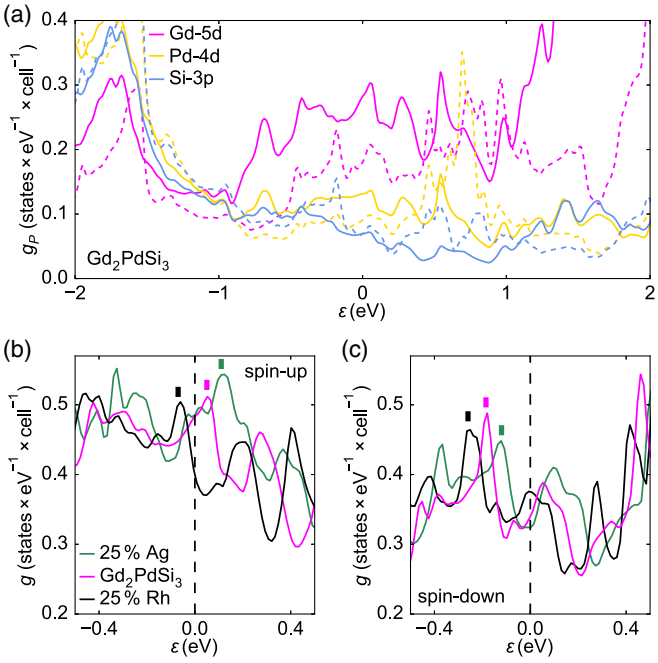

FIG. 4. Density functional theory calculations, neglecting Gd-4f, in the spin-polarized state of pure Gd_2PdSi_3. (a) Partial density of states (P-DOS) $g_P(\varepsilon)$; solid and dashed lines represent spin-up and spin-down bands, respectively. (b),(c) Total DOS $g(\varepsilon)$ for Gd_2PdSi_3 and two doped derivatives. The vertical fat lines are guides to the eye, marking the shift of prominent features in $g(\varepsilon)$ with band filling.

was observed in these calculations, consistent with the rigid band scheme.

The P-DOS in Fig. 4(a) is consistent with previous photoemission work on R_2PdSi_3 ($R = $ Tb, La, Gd) [70] and indicates that Gd-5d orbitals dominate the total DOS at ζ. Sizable Hund's rule coupling within the atomic shell of Gadolinium underpins the large THE and TNE in this material. Considering the giant σ_{xy}^T on the electron-doped side in Fig. 3, it is instructive to examine key material parameters. We draw on experimental data of the carrier mobility (from the normal Hall effect and ρ_{xx}) to estimate the carrier mean free path in stoichiometric Gd_2PdSi_3 [29]. Under the assumption of a twofold spin degenerate spherical (tubular) Fermi surface, $l_{\mathrm{mfp}} = 3.9$ nm (=2.8 nm). Despite disorder, this is comparable to or larger than the characteristic dimensions of the spin texture. Moreover, an order-of-magnitude estimate for the typical Hall conductivity in the intrinsic region yields $\sigma_{xy}^{\mathrm{int}} \approx 950\ \Omega^{-1}\,\mathrm{cm}^{-1}$, not far from the present experimental result [29].

In conclusion, the insights presented here not only demonstrate a giant TNE from skyrmions and establish the validity of Mott's relation for THE and TNE, but also provide a guiding post for driving deeper into the intrinsic regime of THE and TNE for centrosymmetric skyrmion hosts. The present Nernst response of high-density

skyrmion textures in the centrosymmetric magnet Gd_2PdSi_3 is on par with the largest anomalous Nernst signals ever observed in ferromagnets.

We are indebted to H. Ishizuka, M. S. Bahramy, N. Nagaosa, F. Kagawa, and H. Oike for enlightening discussions. L. S. was funded by the German Academic Exchange Service (DAAD) via a PROMOS scholarship awarded by the German Federal Ministry of Education and Research (BMBF), with financial and administrative support by C. Pfleiderer. Work at RIKEN was carried out under JST CREST Grant No. JPMJCR1874 (Japan). M. H. and J. M. were supported as Humboldt/JSPS International Research Fellows (18F18804 and 19F19815, respectively). Contributions by M. Ishida to the graphical presentation of the figures are gratefully acknowledged. This work was performed under the approval of the Photon Factory Program Advisory Committee (Proposal No. 2018G570).

*hirschberger@ap.t.u-tokyo.ac.jp
†Present address: Physik-Department, Technical University of Munich, Garching 85748, Germany.
‡Present address: Department of Physics, Massachusetts Institute of Technology, Cambridge, Massachusetts 02139, USA.
§Present address: Materials Science & Technology Division and Neutron Science Division, Oak Ridge National Laboratory, Oak Ridge, Tennessee 37831, USA.
‖Present address: Institute for Solid State Physics, The University of Tokyo, Kashiwa, Chiba 277-8561, Japan.

[1] A. N. Bogdanov and D. A. Yablonskii, Thermodynamically stable vortices in magnetically ordered crystals. The mixed state of magnets, Zh. Eksp. Teor. Fiz. **95**, 178 (1989) [J. Exp. Theor. Phys. **68**, 101 (1989)], www.jetp.ac.ru/cgi-bin/e/index/e/68/1/p101?a=list.
[2] S. Mühlbauer, B. Binz, F. Jonietz, C. Pfleiderer, A. Rosch, A. Neubauer, R. Georgii, and P. Böni, Skyrmion lattice in a chiral magnet, Science **323**, 915 (2009).
[3] J. Ye, Y. B. Kim, A. J. Millis, B. I. Shraiman, P. Majumdar, and Z. Tešanović, Berry Phase Theory of the Anomalous Hall Effect: Application to Colossal Magnetoresistance Manganites, Phys. Rev. Lett. **83**, 3737 (1999).
[4] K. Ohgushi, S. Murakami, and N. Nagaosa, Spin anisotropy and quantum Hall effect in the Kagomé lattice: Chiral spin state based on a ferromagnet, Phys. Rev. B **62**, R6065 (2000).
[5] R. Shindou and N. Nagaosa, Orbital Ferromagnetism and Anomalous Hall Effect in Antiferromagnets on the Distorted fcc Lattice, Phys. Rev. Lett. **87**, 116801 (2001).
[6] P. Bruno, V. K. Dugaev, and M. Taillefumier, Topological Hall Effect and Berry Phase in Magnetic Nanostructures, Phys. Rev. Lett. **93**, 096806 (2004).
[7] Y. Shiomi, N. Kanazawa, K. Shibata, Y. Onose, and Y. Tokura, Topological Nernst effect in a three-dimensional skyrmion-lattice phase, Phys. Rev. B **88**, 064409 (2013).
[8] Y. P. Mizuta and F. Ishii, Large anomalous Nernst effect in a skyrmion crystal, Sci. Rep. **6**, 28076 (2016).
[9] Y. P. Mizuta, H. Sawahata, and F. Ishii, Large anomalous Nernst coefficient in an oxide skyrmion crystal Chern insulator, Phys. Rev. B **98**, 205125 (2018).
[10] M. Onoda, G. Tatara, and N. Nagaosa, Anomalous Hall effect and skyrmion number in real and momentum spaces, J. Phys. Soc. Jpn. **73**, 2624 (2004).
[11] M. Lee, W. Kang, Y. Onose, Y. Tokura, and N. P. Ong, Unusual Hall Effect Anomaly in MnSi Under Pressure, Phys. Rev. Lett. **102**, 186601 (2009).
[12] A. Neubauer, C. Pfleiderer, B. Binz, A. Rosch, R. Ritz, P. G. Niklowitz, and P. Böni, Topological Hall Effect in the *A* Phase of MnSi, Phys. Rev. Lett. **102**, 186602 (2009).
[13] R. Ritz, M. Halder, C. Franz, A. Bauer, M. Wagner, R. Bamler, A. Rosch, and C. Pfleiderer, Giant generic topological Hall resistivity of MnSi under pressure, Phys. Rev. B **87**, 134424 (2013).
[14] H. Kawamura, Anomalous Hall Effect as a Probe of the Chiral Order in Spin Glasses, Phys. Rev. Lett. **90**, 047202 (2003).
[15] K. Nakazawa, M. Bibes, and H. Kohno, Topological Hall effect from strong to weak coupling, J. Phys. Soc. Jpn. **87**, 033705 (2018).
[16] I. Martin and C. D. Batista, Itinerant Electron-Driven Chiral Magnetic Ordering and Spontaneous Quantum Hall Effect in Triangular Lattice Models, Phys. Rev. Lett. **101**, 156402 (2008).
[17] K. Hamamoto, M. Ezawa, and N. Nagaosa, Quantized topological Hall effect in skyrmion crystal, Phys. Rev. B **92**, 115417 (2015).
[18] J. L. Lado and J. Fernández-Rossier, Quantum anomalous Hall effect in graphene coupled to skyrmions, Phys. Rev. B **92**, 115433 (2015).
[19] B. Göbel, A. Mook, J. Henk, and I. Mertig, The family of topological Hall effects for electrons in skyrmion crystals, Eur. Phys. J. B **91**, 179 (2018).
[20] Z. Wang, Y. Su, S.-Z. Lin, and C. D. Batista, Skyrmion Crystal from RKKY Interaction Mediated by 2D Electron Gas, Phys. Rev. Lett. **124**, 207201 (2020).
[21] J. M. Ziman, *Principles of the Theory of Solids*, 2nd ed. (Cambridge University Press, Cambridge, 1979).
[22] L. Smrčka and P. Středa, Transport coefficients in strong magnetic fields, J. Phys. C **10**, 2153 (1977).
[23] T. Kurumaji, T. Nakajima, M. Hirschberger, A. Kikkawa, Y. Yamasaki, H. Sagayama, H. Nakao, Y. Taguchi, T.-h. Arima, and Y. Tokura, Skyrmion lattice with a giant topological Hall effect in a frustrated triangular-lattice magnet, Science **365**, 914 (2019).
[24] M. Hirschberger, T. Nakajima, S. Gao, L. Peng, A. Kikkawa, T. Kurumaji, M. Kriener, Y. Yamasaki, H. Sagayama, H. Nakao, K. Ohishi, K. Kakurai, Y. Taguchi, X. Yu, T.-h. Arima, and Y. Tokura, Skyrmion phase and competing magnetic orders on a breathing Kagomé lattice, Nat. Commun. **10**, 5831 (2019).
[25] N. D. Khanh, T. Nakajima, X. Z. Yu, S. Gao, K. Shibata, M. Hirschberger, Y. Yamasaki, H. Sagayama, H. Nakao, L. C. Peng, K. Nakajima, R. Takagi, T.-h. Arima, Y. Tokura, and S. Seki, Nanometric square skyrmion lattice in a centrosymmetric tetragonal magnet, Nat. Nanotechnol. **15**, 444 (2020).

[26] D. S. Inosov, D. V. Evtushinsky, A. Koitzsch, V. B. Zabolotnyy, S. V. Borisenko, A. A. Kordyuk, M. Frontzek, M. Loewenhaupt, W. Löser, I. Mazilu, H. Bitterlich, G. Behr, J.-U. Hoffmann, R. Follath, and B. Büchner, Electronic Structure and Nesting-Driven Enhancement of the RKKY Interaction at the Magnetic Ordering Propagation Vector in Gd_2PdSi_3 and Tb_2PdSi_3, Phys. Rev. Lett. **102**, 046401 (2009).

[27] T. Nomoto, T. Koretsune, and R. Arita, Formation mechanism of helical Q structure in Gd-based skyrmion materials, arXiv:2003.13167.

[28] S. R. Saha, H. Sugawara, T. D. Matsuda, H. Sato, R. Mallik, and E. V. Sampathkumaran, Magnetic anisotropy, first-order-like metamagnetic transitions, and large negative magnetoresistance in single-crystal Gd_2PdSi_3, Phys. Rev. B **60**, 12162 (1999).

[29] See the Supplemental Material at http://link.aps.org/supplemental/10.1103/PhysRevLett.125.076602 for sample characterization, details on thermoelectric measurements, supporting resonant x-ray scattering data, and theoretical estimates, which includes Refs. [30–60].

[30] F. Izumi and K. Momma, Three-dimensional visualization in powder diffraction, Solid State Phenom. **130**, 15 (2007).

[31] P. Kotsanidis, J. Yakinthos, and E. Gamari-Seale, Magnetic properties of the ternary rare earth silicides R_2PdSi_3 (R = Pr, Nd, Gd, Tb, Dy, Ho, Er, Tm and Y), J. Magn. Magn. Mater. **87**, 199 (1990).

[32] F. Tang, M. Frontzek, J. Dshemuchadse, T. Leisegang, M. Zschornak, R. Mietrach, J.-U. Hoffmann, W. Löser, S. Gemming, D. C. Meyer, and M. Loewenhaupt, Crystallographic superstructure in $\boldsymbol{R}_2PdSi_3$ compounds ($\boldsymbol{R}$ = heavy rare earth) Phys. Rev. B **84**, 104105 (2011).

[33] Y. Hirokane, Y. Tomioka, Y. Imai, A. Maeda, and Y. Onose, Longitudinal and transverse thermoelectric transport in MnSi, Phys. Rev. B **93**, 014436 (2016).

[34] S. Arsenijević, C. Petrovic, L. Forró, and A. Akrap, Manifestation of the spin textures in the thermopower of MnSi, Europhys. Lett. **103**, 57015 (2013).

[35] J.-G. Cheng, F. Zhou, J.-S. Zhou, J. B. Goodenough, and Y. Sui, Enhanced thermoelectric power near the quantum phase transition in the itinerant-electron ferromagnet MnSi, Phys. Rev. B **82**, 214402 (2010).

[36] P. Blaha, K. Schwarz, F. Tran, R. Laskowski, G. Madsen, and L. Marks, WIEN2k: An APW+lo program for calculating the properties of solids, J. Chem. Phys. **152**, 074101 (2020).

[37] J. P. Perdew, K. Burke, and M. Ernzerhof, Generalized Gradient Approximation Made Simple, Phys. Rev. Lett. **77**, 3865 (1996).

[38] Y. Wang, L. Li, and N. P. Ong, Nernst effect in high-T_c superconductors, Phys. Rev. B **73**, 024510 (2006).

[39] Y. Onose, L. Li, P. Petrovic, and N. P. Ong, Anomalous thermopower and Nernst effect in $CeCoIn_5$: Loss of entropy current in precursor state, Europhys. Lett. **79**, 17006 (2007).

[40] S. Guin, K. Manna, J. Noky, S. Watzman, C. Fu, N. Kumar, W. Schnelle, C. Shekhar, Y. Sun, J. Gooth, and C. Felser, Anomalous Nernst effect beyond the magnetization scaling relation in the ferromagnetic Heusler compound Co_2MnGa, NPG Asia Mater. **11**, 16 (2019).

[41] S. Guin, P. Vir, Y. Zhang, N. Kumar, S. J. Watzman, C. Fu, E. Liu, K. Manna, W. Schnelle, J. Gooth, C. Shekhar, Y. Sun, and C. Felser, Zero-field Nernst effect in a ferromagnetic Kagome-Lattice Weyl-Semimetal $Co_3Sn_2S_2$, Adv. Mater. **31**, 1806622 (2019).

[42] H. Yang, W. You, J. Wang, J. Huang, C. Xi, X. Xu, C. Cao, M. Tian, Z.-A. Xu, J. Dai, and Y. Li, Giant anomalous Nernst effect in the magnetic Weyl semimetal $Co_3Sn_2S_2$, Phys. Rev. Mater. **4**, 024202 (2020).

[43] W.-L. Lee, S. Watauchi, V. Miller, R. J. Cava, and N. P. Ong, Dissipationless anomalous Hall current in the ferromagnetic spinel $CuCr_2Se_{4-x}Br_x$, Science **303**, 1647 (2004).

[44] M. Ikhlas, T. Tomita, T. Koretsune, M.-T. Suzuki, D. Nishio-Hamane, R. Arita, Y. Otani, and S. Nakatsuji, Large anomalous Nernst effect at room temperature in a chiral antiferromagnet, Nat. Phys. **13**, 1085 (2017).

[45] X. Li, L. Xu, L. Ding, J. Wang, M. Shen, X. Lu, Z. Zhu, and K. Behnia, Anomalous Nernst and Righi-Leduc Effects in Mn_3Sn: Berry Curvature and Entropy Flow, Phys. Rev. Lett. **119**, 056601 (2017).

[46] Y. Pu, D. Chiba, F. Matsukura, H. Ohno, and J. Shi, Mott Relation for Anomalous Hall and Nernst Effects in $Ga_{1-x}Mn_xAs$ Ferromagnetic Semiconductors, Phys. Rev. Lett. **101**, 117208 (2008).

[47] R. Ramos, M. H. Aguirre, A. Anadón, J. Blasco, I. Lucas, K. Uchida, P. A. Algarabel, L. Morellón, E. Saitoh, and M. R. Ibarra, Anomalous Nernst effect of Fe_3O_4 single crystal, Phys. Rev. B **90**, 054422 (2014).

[48] M. Frontzek, Magnetic properties of R_2PdSi_3 (R = heavy rare earth) compounds, Ph.D. thesis, Technische Universität Dresden, 2009.

[49] W.-L. Lee, S. Watauchi, V. L. Miller, R. J. Cava, and N. P. Ong, Anomalous Hall Heat Current and Nernst Effect in the $CuCr_2Se_{4-X}Br_X$ Ferromagnet, Phys. Rev. Lett. **93**, 226601 (2004).

[50] K. Everschor, M. Garst, B. Binz, F. Jonietz, S. Mühlbauer, C. Pfleiderer, and A. Rosch, Rotating skyrmion lattices by spin torques and field or temperature gradients, Phys. Rev. B **86**, 054432 (2012).

[51] L. Kong and J. Zang, Dynamics of an Insulating Skyrmion under a Temperature Gradient, Phys. Rev. Lett. **111**, 067203 (2013).

[52] T. Schulz, R. Ritz, A. Bauer, M. Halder, M. Wagner, C. Franz, C. Pfleiderer, K. Everschor, M. Garst, and A. Rosch, Emergent electrodynamics of skyrmions in a chiral magnet, Nat. Phys. **8**, 301 (2012).

[53] S. Hoshino and N. Nagaosa, Theory of the magnetic skyrmion glass, Phys. Rev. B **97**, 024413 (2018).

[54] L. Taillefer, G. Lonzarich, and P. Strange, The band magnetism of MnSi, J. Magn. Magn. Mater. **5457**, 957 (1986).

[55] C. Pfleiderer, G. J. McMullan, S. R. Julian, and G. G. Lonzarich, Magnetic quantum phase transition in MnSi under hydrostatic pressure, Phys. Rev. B **55**, 8330 (1997).

[56] S. Onoda, N. Sugimoto, and N. Nagaosa, Quantum transport theory of anomalous electric, thermoelectric, and thermal Hall effects in ferromagnets, Phys. Rev. B **77**, 165103 (2008).

[57] H. Chen, Q. Niu, and A. H. MacDonald, Anomalous Hall Effect Arising from Noncollinear Antiferromagnetism, Phys. Rev. Lett. **112**, 017205 (2014).

[58] S. Nakatsuji, N. Kiyohara, and T. Higo, Large anomalous Hall effect in a non-collinear antiferromagnet at room temperature, Nature (London) **527**, 212 (2015).

[59] L. Ye, M. Kang, J. Liu, F. von Cube, C. Wicker, T. Suzuki, C. Jozwiak, A. Bostwick, E. Rotenberg, D. Bell, L. Fu, R. Comin, and J. Checkelsky, Massive Dirac fermions in a ferromagnetic Kagome metal, Nature (London) **555**, 638 (2018).

[60] D. Gosálbez-Martínez, I. Souza, and D. Vanderbilt, Chiral degeneracies and Fermi-surface Chern numbers in bcc Fe, Phys. Rev. B **92**, 085138 (2015).

[61] M. Hirschberger, T. Nakajima, M. Kriener, T. Kurumaji, L. Spitz, S. Gao, A. Kikkawa, Y. Yamasaki, H. Sagayama, H. Nakao, S. Ohira-Kawamura, S. Taguchi, T.-H. Arima, and Y. Tokura, High-field depinned phase and planar Hall effect in skyrmion-host Gd_2PdSi_3, Phys. Rev. B **101**, 220401(R) (2020).

[62] N. Hanasaki, K. Sano, Y. Onose, T. Ohtsuka, S. Iguchi, I. Kézsmárki, S. Miyasaka, S. Onoda, N. Nagaosa, and Y. Tokura, Anomalous Nernst Effects in Pyrochlore Molybdates with Spin Chirality, Phys. Rev. Lett. **100**, 106601 (2008).

[63] N. Kanazawa, Y. Onose, T. Arima, D. Okuyama, K. Ohoyama, S. Wakimoto, K. Kakurai, S. Ishiwata, and Y. Tokura, Large Topological Hall Effect in a Short-Period Helimagnet MnGe, Phys. Rev. Lett. **106**, 156603 (2011).

[64] R. Schlitz, P. Swekis, A. Markou, H. Reichlova, M. Lammel, J. Gayles, A. Thomas, K. Nielsch, C. Felser, and S. T. B. Goennenwein, All electrical access to topological transport features in $Mn_{1.8}PtSn$ films, Nano Lett. **19**, 2366 (2019).

[65] L. Ding, J. Koo, L. Xu, X. Li, X. Lu, L. Zhao, Q. Wang, Q. Yin, H. Lei, B. Yan, Z. Zhu, and K. Behnia, Intrinsic Anomalous Nernst Effect Amplified by Disorder in a Half-Metallic Semimetal, Phys. Rev. X **9**, 041061 (2019).

[66] A. Sakai, Y. P. Mizuta, A. A. Nugroho, R. Sihombing, T. Koretsune, M.-T. Suzuki, N. Takemori, R. Ishii, D. Nishio-Hamane, R. Arita, P. Goswami, and S. Nakatsuji, Giant anomalous Nernst effect and quantum-critical scaling in a ferromagnetic semimetal, Nat. Phys. **14**, 1119 (2018).

[67] T. Miyasato, N. Abe, T. Fujii, A. Asamitsu, S. Onoda, Y. Onose, N. Nagaosa, and Y. Tokura, Crossover Behavior of the Anomalous Hall Effect and Anomalous Nernst Effect in Itinerant Ferromagnets, Phys. Rev. Lett. **99**, 086602 (2007).

[68] S. J. Watzman, R. A. Duine, Y. Tserkovnyak, S. R. Boona, H. Jin, A. Prakash, Y. Zheng, and J. P. Heremans, Magnon-drag thermopower and Nernst coefficient in Fe, Co, and Ni, Phys. Rev. B **94**, 144407 (2016).

[69] J. Weischenberg, F. Freimuth, S. Blügel, and Y. Mokrousov, Scattering-independent anomalous Nernst effect in ferromagnets, Phys. Rev. B **87**, 060406(R) (2013).

[70] A. N. Chaika, A. M. Ionov, M. Busse, S. L. Molodtsov, S. Majumdar, G. Behr, E. V. Sampathkumaran, W. Schneider, and C. Laubschat, Electronic structure of R_2PdSi_3 (R = La, Ce, Gd, and Tb) compounds, Phys. Rev. B **64**, 125121 (2001).

[71] R. Mallik and E. V. Sampathkumaran, Magnetic behavior of the alloys $(Ce_{1-x}Y_x)_2PdSi_3$, J. Magn. Magn. Mater. **164**, L13 (1996).

[72] M. Guo, Y. Ou, Y. Xu, Y. Feng, G. Jiang, K. He, X. Ma, Q.-K. Xue, and Y. Wang, Ambi-polar anomalous Nernst effect in a magnetic topological insulator, New J. Phys. **19**, 113009 (2017).